Picosecond Raman scattering studies of carrier dynamics in $In_xGa_{1-x}As_{1-y}N_y$

2004 J. Phys.: Condens. Matter 16 S3333

(http://iopscience.iop.org/0953-8984/16/31/022)

INSTITUTE OF PHYSICS PUBLISHING JOURNAL OF PHYSICS: CONDENSED MATTER

J. Phys.: Condens. Matter **16** (2004) S3333–S3343 PII: S0953-8984(04)74835-3

Picosecond Raman scattering studies of carrier dynamics in $In_xGa_{1-x}As_{1-y}N_y$

K T Tsen

Department of Physics and Astronomy, Arizona State University, Tempe, AZ 85287, USA

E-mail: tsen@asu.edu

Received 14 January 2004
Published 23 July 2004
Online at stacks.iop.org/JPhysCM/16/S3333
doi:10.1088/0953-8984/16/31/022

Abstract

Picosecond Raman spectroscopy has been used to study non-equilibrium electron distributions and energy loss rate in a metal–organic-chemical-vapour-deposition-grown $In_xGa_{1-x}As_{1-y}N_y$ ($x = 0.03$ and $y = 0.01$) epilayer grown on GaAs substrate. It is demonstrated that for the photoexcited electron–hole pair density of $n \cong 10^{18}$ cm^{-3} electron distributions can be described very well by Fermi–Dirac distributions with effective electron temperatures substantially higher than the lattice temperature. From the measurement of electron temperature as a function of the pulse width of the excitation laser, the energy loss rate in $In_xGa_{1-x}As_{1-y}N_y$ is estimated to be about 64 meV ps^{-1}. These experimental results are compared with those of GaAs and important implications are given.

1. Introduction

Recently, the successful fabrication of operational InGaAsN/GaAs laser diodes by using gas-source molecular beam epitaxy (GSMBE) [1–3], chemical beam epitaxy (CBE) [4] and metal–organic chemical vapour deposition (MOCVD) [5, 6] techniques has attracted a lot of attention. The quaternary InGaAsN alloy system, because of its ability to remain lattice matched to other semiconductors such as GaAs, Ge and InP [7], has been predicted to have superior temperature characteristics compared to the InGaAsP alloy system. InGaAsN alloys have also been predicted to have great potential for multi-bandgap solar cells [8, 9]. It was found that the minority-carrier diffusion length increases substantially after post-growth annealing in a nitrogen ambient, and as a result the quantum efficiency in such solar cells can be as high as 70%. More recently, Mair *et al* [10] have reported the results of time-resolved photoluminescence spectroscopy studies of an InGaAsN epilayer. These authors concluded that the localized states in InGaAsN, which arose from alloy fluctuations, played an important role in the decay of the photoluminescence intensity. Paramount knowledge of carrier dynamics is essential

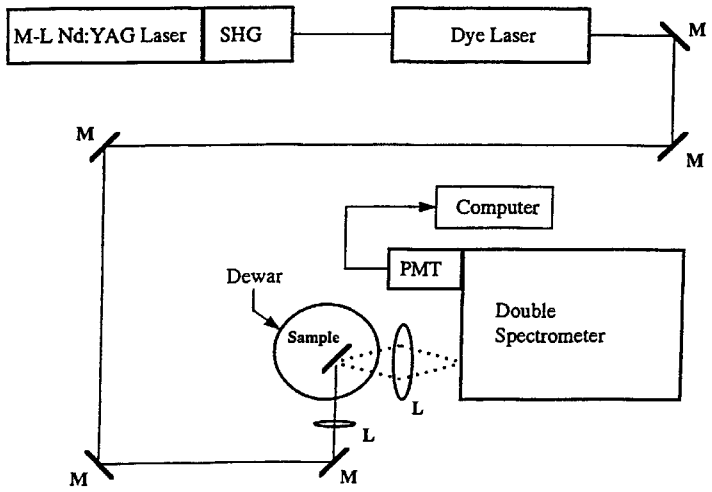

Figure 1. The experimental set-up for transient (single-pulse) picosecond Raman scattering studies of electron transient transport in semiconductors. SHG, second-harmonic generation system; M, mirror; L, lens; PMT, photomultiplier tube. For transient experiments, the same laser pulse is used for both excitation of electron–hole pairs and detection of their transport properties.

for design engineers to devise an efficient semiconductor device. In this paper, we report our results on carrier dynamics of an InGaAsN epilayer grown on GaAs substrate by using single-pulse Raman spectroscopy on a picosecond timescale.

2. Sample and experimental technique

The InGaAsN epilayer studied in this work was grown by MOCVD on a semi-insulating GaAs substrate and terminated with a 5 nm thick GaAs cap. The nominal In and N molar fractions were 0.03 and 0.01, respectively. The In/N incorporation ratio of three has been shown to provide a lattice match to GaAs. As grown, the undoped InGaAsN film was p type. After growth, the sample was annealed at 600 °C for 30 min in a nitrogen ambient in order to improve the electrical as well as optical properties of the material.

The excitation source was a double-jet DCM dye laser [11] synchronously pumped by the second-harmonic output of a continuous wave (cw) mode-locked yttrium–aluminium–garnet (YAlG) laser operating at a repetition rate of 76 MHz, which is shown in figure 1. The photon energy was chosen to be $\hbar\omega_{\rm i} = 1.931$ eV. The pulse width of the dye laser can be tuned almost continuously from 1 to 5 ps by changing the concentration of the saturable absorber and the birefringence filter. Single-particle scattering (SPS) spectra were taken in the $Z(X, Y)\bar{Z}$ scattering geometry so that only the SPS spectra associated with spin-density fluctuations (SDFs) were measured [12, 13]. Here, $X = (100)$, $Y = (010)$ and $Z = (001)$. The photoexcited electron–hole pair density was estimated to be $n \cong 1 \times 10^{18}$ cm^{-3} by fitting the luminescence spectrum of the E_0 bandgap of InGaAsN [14]. The backward-scattered Raman signal was collected and analysed by a standard Raman system consisting of a double spectrometer and a low-background-count photomultiplier. All of the SPS spectra presented here were taken at $T = 300$ K.

2.1. Raman spectroscopy in semiconductors

We first present a brief theory of Raman scattering from carriers in semiconductors, which will be particularly useful for situations where electron distributions are non-equilibrium such

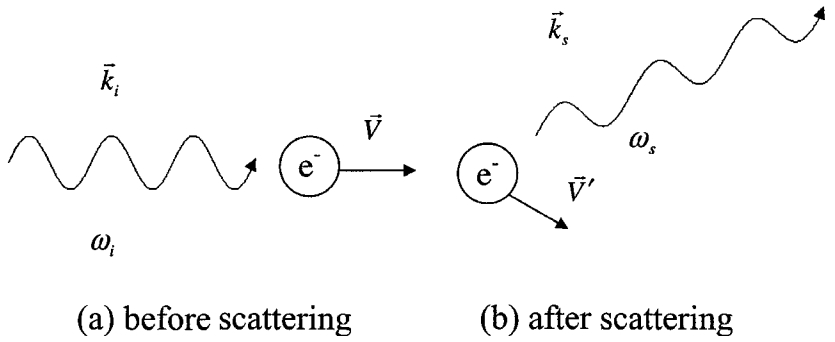

Figure 2. A simple model—Compton scattering, demonstrating how the electron distribution in semiconductors can be directly probed by Raman spectroscopy.

as in our current situation; and then we discuss on the theory of Raman scattering by lattice vibrations in semiconductors.

2.1.1. Theory of Raman scattering from carriers in semiconductors.

(a) A simple model. In order to understand how Raman spectroscopy can be used to probe the electron distribution function in semiconductors, we start with the simplest physical concept—Compton scattering. As shown in figure 2, let us consider that an incident photon with wavevector $\vec{k}_\mathrm{i}$ and angular frequency ω_i is interacting with an electron of mass m_e^* travelling at a velocity $\vec{V}$. After the scattering event, the scattered photon is characterized by wavevector $\vec{k}_\mathrm{s}$ and angular frequency ω_s. The scattered electron is then moving at a velocity $\vec{V}'$. From the conservation of energy and momentum, we can write down the following equations:

$$\hbar\omega_\mathrm{i} + \tfrac{1}{2}m_\mathrm{e}^*\vec{V}^2 = \hbar\omega_\mathrm{s} + \tfrac{1}{2}m_\mathrm{e}^*\vec{V}'^2 \tag{1}$$

$$\hbar\vec{k}_\mathrm{i} + m_\mathrm{e}^*\vec{V} = \hbar\vec{k}_\mathrm{s} + m_\mathrm{e}^*\vec{V}'. \tag{2}$$

If we define the energy transfer and the wavevector transfer of the photon to be $\omega \equiv \omega_\mathrm{i} - \omega_\mathrm{s}$, and $\vec{q} \equiv \vec{k}_\mathrm{i} - \vec{k}_\mathrm{s}$ respectively, then from equations (1) and (2) we have

$$\omega = \vec{V}\cdot\vec{q} + \frac{\hbar\vec{q}^2}{2m_\mathrm{e}^*}. \tag{3}$$

This important equation states that the energy transfer of the incident photon is (apart from a constant term, $\frac{\hbar\vec{q}^2}{2m_\mathrm{e}^*}$) directly proportional to the electron velocity along the direction of wavevector transfer. In other words, it implies that Raman scattering intensity, measured at an angular frequency ω, is proportional to the number of electrons that have a velocity component along the direction of wavevector transfer given by equation (3), irrespective of their velocity components perpendicular to $\vec{q}$.

Therefore, if the electron distribution function is Maxwell–Boltzmann-like, then the lineshape of the Raman scattering spectrum will be Gaussian-like, centred around $\omega \cong 0$, whereas a drifted Maxwell–Boltzmann distribution with an electron drift velocity $\vec{V}_\mathrm{d}$ will result in a Raman scattering spectrum which is a shifted Gaussian centred around $\omega \cong \vec{q}\cdot\vec{V}_\mathrm{d}$.

However, we note that, strictly speaking, this simple picture is only correct for a system of a non-interacting electron gas in vacuum. For an electron gas in a semiconductor such as GaAs or GaN, many-body effects and the effects of band structure have to be considered. The former is usually taken into account by the random-phase approximation (RPA) [15] and the latter by sophisticated band structure calculations such as $\vec{k}\cdot\vec{p}$ approximation [16] or pseudopotential calculations [17].

(b) A full quantum mechanical approach. We now use a quantum mechanical method to calculate the Raman scattering cross section or SPS spectrum for a single-component plasma in a direct bandgap semiconductor such as GaAs, probed by an ultrafast laser having pulse width $t_{\rm p}$. For simplicity, we assume that the probe pulse is a square pulse from $-\frac{t_{\rm p}}{2}$ to $+\frac{t_{\rm p}}{2}$ and the electron elastic scattering is the dominant scattering process in the solid state system.

We start with a typical electron–photon interaction Hamiltonian which has been shown in the equilibrium case to be [18]

$$H = H_0 + \sum_i \left[\frac{-e}{2m_{\rm e}^* c}[\vec{p}_i \cdot \vec{A}(\vec{r}_i) + \vec{A}(\vec{r}_i) \cdot \vec{p}_i] + \frac{e^2}{2m_{\rm e}^* c}\vec{A}^2(\vec{r}_i) \right] \equiv H_0 + H_1 + H_2; \tag{4}$$

where H_0 is the total Hamiltonian of the system in the absence of the radiation field; e is the charge of an electron; c is the speed of light; $\vec{p}$ is the electron momentum; $\sum_i$ refers to summation over electrons; the second and third terms describe the interactions of electrons with radiation field; $\vec{A}$ is the vector potential of the radiation field,

$$\vec{A}(\vec{r}_i) \equiv \frac{1}{\sqrt{V}} \sum_j \left(\frac{2\pi\hbar c^2}{\omega_j} \right)^{1/2} \left({\rm e}^{{\rm i}\vec{k}_j \cdot \vec{r}_i} b_{\vec{k}_j} + {\rm e}^{-{\rm i}\vec{k}_j \cdot \vec{r}_i} b_{\vec{k}_j}^+ \right) \hat{e}_j; \tag{5}$$

where V is the volume of the semiconductor; $b_{\vec{k}_j}$, $b_{\vec{k}_j}^+$ are photon annihilation and creation operators, respectively. Since the vector potential $\vec{A}$ is a linear combination of photon creation and annihilation operators, and the Raman scattering process involves the annihilation of an incident photon and the creation of a scattered photon, $\vec{p} \cdot \vec{A}$ and $\vec{A} \cdot \vec{p}$ terms in equation (4) will contribute to the scattering matrix element in the second order and $\vec{A}^2$ terms contribute in the first order in the perturbation-theory calculations of Raman scattering cross section.

The single-particle scattering (SPS) cross section associated with spin-density fluctuations (SDFs) for a single-component plasma in a direct bandgap semiconductor such as GaAs, probed by an ultrafast laser having pulse width $t_{\rm p}$ and when elastic scattering is dominant, can be shown to be given by [19–21]

$$\begin{aligned} \left(\frac{{\rm d}^2\sigma}{{\rm d}\omega\,{\rm d}\Omega} \right)_{\rm SDF} &= C \cdot \sum_{\vec{p}} -n(\vec{p})[1 - n(\vec{p} + \vec{q})](\hat{e}_{\rm i} \times \hat{e}_{\rm s})^2 \\ &\quad \cdot \int_{-\infty}^{\infty} {\rm d}\omega' \int_{-t_{\rm p}/2}^{t_{\rm p}/2} {\rm d}t \int_{-t_{\rm p}/2-t}^{t_{\rm p}/2-t} {\rm d}t'\, {\rm e}^{{\rm i}(\omega-\omega')t'} S_{\rm p}(t, \omega_{\rm i}) S_{\rm p}^*(t' + t, \omega_{\rm i}) \\ &\quad \cdot {\rm Im}\left\{ \frac{1}{\hbar\omega' + \varepsilon_{\vec{p}} - \varepsilon_{\vec{p}+\vec{q}} + {\rm i}\hbar/\tau} \left[1 - \frac{{\rm i}\hbar}{\tau} \left\langle \frac{1}{\hbar\omega' + \varepsilon_{\vec{p}} - \varepsilon_{\vec{p}+\vec{q}} + {\rm i}\hbar/\tau} \right\rangle_{\Omega_{\vec{p}}} \right]^{-1} \right\}; \end{aligned} \tag{6}$$

where C is a constant; $n(\vec{p})$ is the electron distribution function; $\hat{e}_{\rm i}$ and $\hat{e}_{\rm s}$ are polarization vectors of the incident and scattered light, respectively; $\omega_{\rm i}$ and $\omega_{\rm s}$ are angular frequencies of the incident and scattered light, respectively; $\omega \equiv \omega_{\rm i} - \omega_{\rm s}$; $t_{\rm p}$ is the pulse width of the probe laser; $\varepsilon_{\vec{p}}$ is the electron energy at $\vec{p}$; τ is the electron collision time; $\Omega_{\vec{p}}$ represents an average over the solid angle in the momentum space and

$$\begin{aligned} S_{\rm p}(t, \omega_{\rm i}) \equiv -\Bigg\{ \left(\frac{P^2}{3m_{\rm e}^*} \right) \cdot \sum_{n=1}^{3} A_{\rm s}(n) \\ \cdot \frac{\hbar\omega_{\rm i} - {\rm e}^{\frac{{\rm i}}{\hbar}E_{g_n}(t+t_{\rm p}/2)}\{\hbar\omega_{\rm i}\cos[\omega_{\rm i}(t + t_{\rm p}/2)] - {\rm i}E_{g_n}\sin[\omega_{\rm i}(t + t_{\rm p}/2)]\}}{(E_{g_n} - {\rm i}\Gamma_n)^2 - (\hbar\omega_{\rm i})^2} \Bigg\}; \end{aligned}$$

where $m_{\rm e}^*$ is the effective mass of the electron on the conduction band; $A_{\rm s}(1) = A_{\rm s}(2) = 1$ and $A_{\rm s}(3) = -2$. $\Gamma_1, \Gamma_2, \Gamma_3$ are the damping constants involved in the Raman scattering processes.

E_{g_1}, E_{g_2} and E_{g_3} are the energy differences between the conduction band and the heavy-hole, light-hole and split-off-hole bands evaluated at wavevector $\vec{k}$, respectively. $P \equiv -\mathrm{i}\langle S|p_z|Z\rangle$ is the momentum matrix element between the conduction and valence bands at the Γ-point in Kane's notations [22].

We note that in the limit of very long probe pulse ($t_\mathrm{p} \to \infty$) and equilibrium electron distributions our results can be shown to reduce to expressions previously given for the Raman scattering cross section in the equilibrium case [23].

It is very instructive to note that if we assume that the pulse width of the probe pulse is sufficiently wide, collision effects are negligible, the electron distribution function is non-degenerate and the term involving matrix elements—S_p—does not depend upon the electron momentum, equation (6) can be shown to become

$$\left(\frac{\mathrm{d}^2\sigma}{\mathrm{d}\omega\,\mathrm{d}\Omega}\right)_\mathrm{SDF} \propto \int \mathrm{d}^3p \cdot n(\vec{p}) \cdot \delta\left[\omega - \vec{V}\cdot\vec{q} - \frac{\hbar q^2}{2m_\mathrm{e}^*}\right]; \tag{7}$$

here, the δ-function in equation (7) ensures that both the energy and momentum are conserved.

We note that equation (7) shows that the measured Raman scattering cross section at a given solid angle dΩ (which determines $\vec{q}$) provides *direct* information about the electron distribution function in the direction of wavevector transfer $\vec{q}$, in agreement with the simple classical picture.

One intriguing feature for probing carrier distributions with Raman spectroscopy is that since Raman scattering cross section is inversely proportional to the square of the effective mass of the carrier, it preferentially probes electron distribution even if holes are simultaneously present. This unique feature makes the interpretation of electron distribution in Raman scattering experiments much simpler than those of other techniques.

2.1.2. Theory of Raman scattering by lattice vibrations in semiconductors. Consider an incident laser beam of angular frequency ω_i which is scattered by a semiconductor and the scattered radiation is analysed spectroscopically, as shown in figure 3. In general, the scattered radiation consists of a laser beam of angular frequency ω_i accompanied by weaker lines of angular frequencies $\omega_\mathrm{i} \pm \omega$. The line at an angular frequency $\omega_\mathrm{i} - \omega$ is called a Stokes line, whereas that at an angular frequency $\omega_\mathrm{i} + \omega$ is usually referred to as an anti-Stokes line. The important aspect is that the angular frequency shifts ω are independent of ω_i. In this way, this phenomenon differs from that of luminescence, in which it is the angular frequency of the emitted light that is independent of ω_i. The effect just described is called the Raman effect. It was predicted by Smekal [24] and is implicit in the radiation theory of Kramers and Heisenberg [25]. It was discovered experimentally by Raman [26] and by Landsberg and Mandel'shtam [27] in 1928. It can be understood as an inelastic scattering of light in which an internal form of motion of the scattering system is either excited or absorbed during the process.

(a) A simple classical theory. Let us imagine that we have a crystalline lattice having an internal mode of vibration characterized by a normal coordinate

$$Q = Q_0 \cos\omega t; \tag{8}$$

the electronic polarizability α is generally a function of Q and, since in general, $\omega \ll \omega_\mathrm{i}$, at each instant we can regard Q as fixed compared with the variation of the external field $\vec{E}$, i.e., at angular frequency ω_i the induced dipole moment $\vec{P}$ is

$$\vec{P} = \alpha\vec{E} = \alpha(Q)\vec{E}. \tag{9}$$

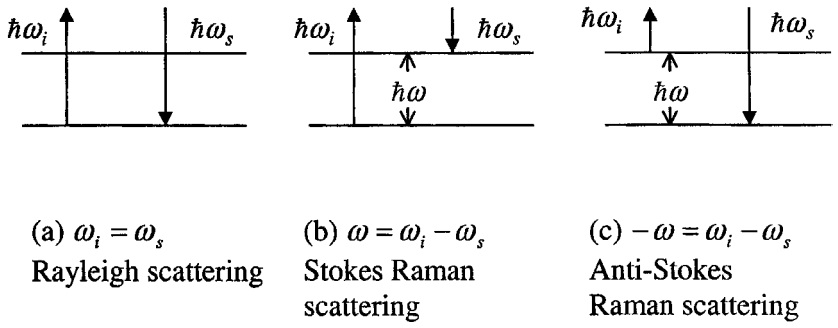

Figure 3. A diagram showing (a) the Rayleigh scattering process; (b) the Stokes Raman scattering process and (c) the anti-Stokes Raman scattering process.

Let $\alpha_0 = \alpha(0)$ be the polarizability in the absence of any excitation. We can write

$$\begin{aligned}\alpha(Q) &= \alpha_0 + \left(\frac{\partial\alpha}{\partial Q}\right)_0 Q + \frac{1}{2}\left(\frac{\partial^2\alpha}{\partial Q^2}\right)_0 Q^2 + \cdots \\ &= \alpha_0 + \alpha_1 Q + \tfrac{1}{2}\alpha_2 Q^2 + \cdots; \end{aligned} \tag{10}$$

where $\left[\frac{\partial\alpha}{\partial Q}\right]_0 \equiv \alpha_1$; $\left[\frac{\partial^2\alpha}{\partial Q^2}\right]_0 \equiv \alpha_2$ and the derivative is to be evaluated at zero excitation field.

If we assume that $\vec{E} = \vec{E}_0 \cos\omega_i t$, we find that

$$\begin{aligned}\vec{P}(t) = \left(\alpha_0\vec{E}_0 + \frac{1}{4}\alpha_2 Q_0^2\vec{E}_0\right)\cos\omega_i t + \frac{\vec{E}_0}{2}\alpha_1 Q_0[\cos(\omega_i+\omega)t + \cos(\omega_i-\omega)t] \\ + \tfrac{1}{8}\alpha_2 Q_0^2\vec{E}_0[\cos(\omega_i+2\omega) + \cos(\omega_i-2\omega)] + \cdots. \end{aligned} \tag{11}$$

For an oscillating dipole moment, the magnetic and electric fields of emitted electromagnetic wave are given by [28]

$$\vec{B} = \frac{1}{c^2 r}\left[\frac{\partial^2\vec{P}\left(t-\frac{r}{c}\right)}{\partial^2 t}\right]\times\hat{n}; \tag{12a}$$

and

$$\vec{E} = \vec{B}\times\hat{n}, \tag{12b}$$

where $\vec{r}$ is the position vector connecting the centre of dipole moment to the point of observation, and $\hat{n} = \vec{r}/|\vec{r}|$.

Therefore, the first term in equation (11) gives rise to Rayleigh scattering; the second term gives the anti-Stokes and Stokes first order Raman lines, respectively; the third term takes into account the anti-Stokes and Stokes second order Raman lines, and so on. We notice that in equation (11) the intensities of the Stokes and anti-Stokes lines are equal. This is because all classical theories neglect the possibility of spontaneous emission.

(b) A quantum mechanical theory. In the quantum mechanical treatment of scattering of light by lattice vibrations, we consider the total Hamiltonian of the system, including the radiation field:

$$H = H_0' + H_{\text{el–ph}} + H'; \tag{13}$$

where H_0' includes contributions from the electronic system, lattice vibrations (or phonons) and radiation field; $H_{\text{el–ph}} = -e\varphi(\vec{r}_i)$ describes the interaction of electrons with phonons;

$\varphi(\vec{r}_i)$ is the potential due to, say, deformation potential and/or Fröhlich interactions and

$$H' = \sum_i \frac{-e}{2m_e c}\left[\vec{A}(\vec{r}_i)\cdot\vec{p}_i + \vec{p}_i\cdot\vec{A}(\vec{r}_i)\right] + \sum_i \frac{e^2}{2m_e c^2}\vec{A}^2(\vec{r}_i)$$
$$= \sum_i \frac{-e}{m_e c}[\vec{p}_i\cdot\vec{A}(\vec{r}_i)] + \sum_i \frac{e^2}{2m_e c^2}\vec{A}^2(\vec{r}_i) \equiv H_1' + H_2'; \tag{14}$$

takes into account the electron–photon interactions, where $\vec{A}(\vec{r}_i)$ is the vector potential of the radiation field given by equation (5).

We notice that for a typical Raman scattering process in which $\omega_i \gg \omega$ photons do not interact directly with phonons, but through electron–phonon interactions, i.e., the H_{el-ph} term in the total Hamiltonian. Since the Raman scattering process involves the annihilation of an incident photon and the creation of a scattered photon, $\vec{p}\cdot\vec{A}$ and $\vec{A}\cdot\vec{p}$ terms in equation (14) will contribute to the scattering matrix element in the third order and $\vec{A}^2$ terms contribute in the second order in the perturbation-theory calculations of Raman scattering cross section. If we neglect non-linear processes, then only $\vec{p}\cdot\vec{A}$ and $\vec{A}\cdot\vec{p}$ terms in equation (14) are important and need to be considered.

From the time-dependent perturbation theory and Fermi golden rule, we obtain for the scattering probability (which is proportional to the Raman scattering cross section) for a one-phonon Stokes Raman process [29]

$$P(\omega_s) = \frac{2\pi}{\hbar}\left|\sum_{n,n'}\frac{\langle i|H_1'|n\rangle\langle n|H_{el-ph}|n'\rangle\langle n'|H_1'|i\rangle}{[\hbar\omega_i - (E_n - E_i)][\hbar\omega_i - \hbar\omega - (E_{n'} - E_i)]}\right.$$
$$+\sum_{n,n'}\frac{\langle i|H_1'|n\rangle\langle n|H_1'|n'\rangle\langle n'|H_{el-ph}|i\rangle}{[\hbar\omega_i - (E_n - E_i)][\hbar\omega_i - \hbar\omega_s - (E_{n'} - E_i)]}$$
$$+\sum_{n,n'}\frac{\langle i|H_1'|n\rangle\langle n|H_{el-ph}|n'\rangle\langle n'|H_1'|i\rangle}{[-\hbar\omega_s - (E_n - E_i)][-\hbar\omega_s - \hbar\omega - (E_{n'} - E_i)]}$$
$$+\sum_{n,n'}\frac{\langle i|H_1'|n\rangle\langle n|H_1'|n'\rangle\langle n'|H_{el-ph}|i\rangle}{[-\hbar\omega_s - (E_n - E_i)][-\hbar\omega_i + \hbar\omega - (E_{n'} - E_i)]}$$
$$+\sum_{n,n'}\frac{\langle i|H_{el-ph}|n\rangle\langle n|H_1'|n'\rangle\langle n'|H_1'|i\rangle}{[-\hbar\omega - (E_n - E_i)][-\hbar\omega + \hbar\omega_i - (E_{n'} - E_i)]}$$
$$\left.+\sum_{n,n'}\frac{\langle i|H_{el-ph}|n\rangle\langle n|H_1'|n'\rangle\langle n'|H_1'|i\rangle}{[-\hbar\omega - (E_n - E_i)][-\hbar\omega - \hbar\omega_s - (E_{n'} - E_i)]}\right|^2$$
$$\times\,\delta(\hbar\omega_i - \hbar\omega_s - \hbar\omega); \tag{15}$$

where $|i\rangle$ is the initial state of the system and E_i is its energy; $|n\rangle$ and $|n'\rangle$ are intermediate states with energies E_n and $E_{n'}$, respectively.

We note that there are three processes involved in one-phonon Raman scattering: the incident photon is annihilated; the scattered photon is emitted; and a phonon is annihilated (or created). Since these three processes can occur in any time order in the time-dependent perturbation-theory calculations of scattering probability, we expect that there will be six terms or contributions to $P(\omega_s)$, which is consistent with equation (15). The δ-function here ensures that energy is conserved in the Raman scattering process.

One important advantage of probing non-equilibrium excitations with Raman spectroscopy in semiconductors is that, since it detects a Raman signal only when excitation photons are present, its time resolution is essentially limited by the pulse width of the excitation

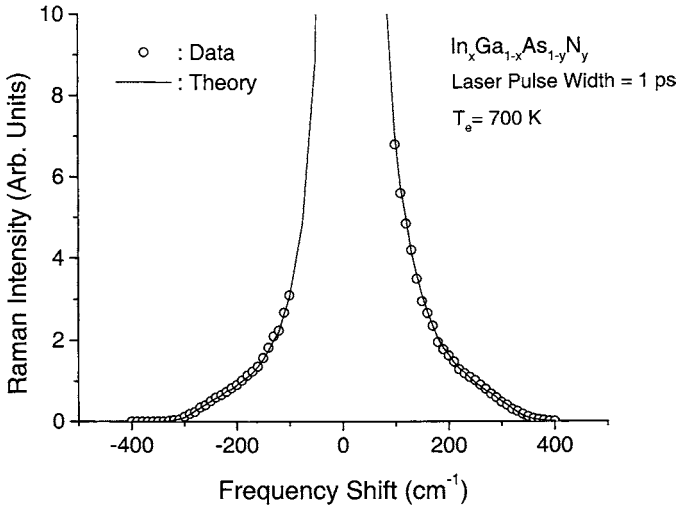

Figure 4. SPS spectrum (open circles) for an InGaAsN sample, taken with an ultrafast laser having 1 ps pulse width and photon energy $\hbar\omega_i = 1.931$ eV. The photoexcited electron-pair density is $n \cong 1 \times 10^{18}$ cm^{-3}. The SPS spectrum is fitted by equation (6) (solid curve). The electron distribution is assumed to be a Fermi–Dirac function. The best fitting parameter set is $T_e = (700 \pm 35)$ K, $\tau = (10 \pm 1)$ fs and $\Gamma = 15$ meV.

laser and not by the response of the detection system. This explains why our detection system has a time resolution of the order of a nanosecond whereas the time resolution in our Raman experiments is typically on the scale of a picosecond.

3. Experimental results and analysis

Figure 4 show a typical SPS spectrum for an InGaAsN sample taken with photon energy $\hbar\omega_i = 1.931$ eV, an electron–hole pair density of $n \cong 1 \times 10^{18}$ cm^{-3} and a laser pulse width of 1 ps and at $T = 300$ K.

By using equation (6) and assuming that the electron distribution is a Fermi–Dirac function with an effective electron temperature much higher than the lattice temperature, we will be able to fit the SPS of figure 4 pretty well. This is shown in figure 4. The parameter set that best fits the experimental results is $T_e = (700 \pm 35)$ K, $\tau = (10 \pm 1)$ fs and $\Gamma_1 = \Gamma_2 = \Gamma_3 = 15$ meV. The quality of the fit suggests that under our experimental conditions electron distributions can be very well described by Fermi–Dirac functions with an effective electron temperature much higher than the lattice temperature. We notice that the damping constants involved in the Raman scattering processes (Γ) are very close to the value (13 meV) that has been obtained from the analysis of resonance Raman profiles in the equilibrium case [30]. We notice that alternatively a quantum mechanical Monte Carlo simulation can be performed under our experimental conditions to obtain the non-equilibrium electron distributions and then compare them with our experimental results; however, the simulation requires input parameters such as electron–phonon scattering rates, effective masses of the electron and hole and the band structure of the semiconductor. This information is not usually readily available for a new class of semiconductors such as that investigated here. Therefore, the simulation can be in principle performed on such a system but the results will not be very useful because of the requirements of several input parameters.

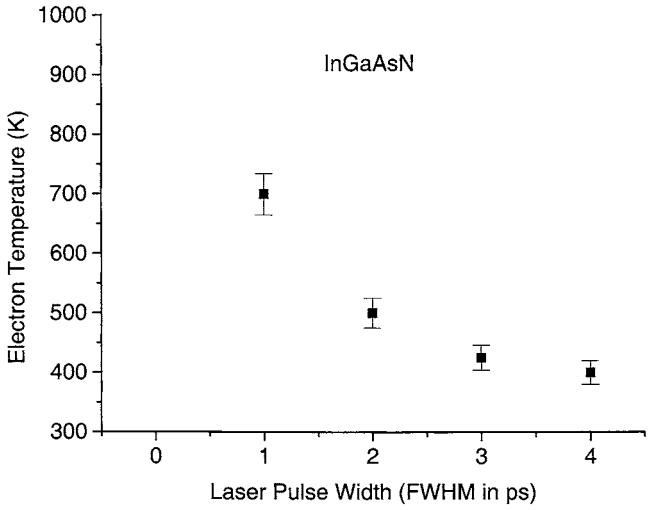

Figure 5. The deduced electron temperature is plotted as a function of the laser pulse width for an InGaAsN sample. From the data, the electron energy loss rate is estimated to be (64 ± 6) meV ps^{-1}.

Figure 5 shows the effective electron temperature obtained in this way as a function of the pulse width of the excitation laser, ranging from 1 to 4 ps. This plot demonstrates that the effective electron temperature decreases from 700 to 400 K when we increase the laser pulse width from 1 to 4 ps. Using the result of Kim and Yu [31, 32], which states that the electron effective temperature determined with a single pulse of FWHM of δt is equal to the temperature of the electron after cooling for an equivalent duration $0.4\delta t$ when excited by an infinitely short pulse, we estimate that the electron cooling rate (energy loss rate) is equal to $\left[\frac{3}{2}(700\text{–}500)\ k_B\right]/(0.4)$ ps, where k_B is the Boltzmann constant, or about (64 ± 6) meV ps^{-1}.

In order to get a better insight into our experimental results we have also carried out similar experimental measurements on a molecular-beam-epitaxy- (MBE-) grown GaAs sample. The results are shown in figure 6. These results indicate that within our experimental uncertainty the energy loss rate for an InGaAsN sample is the same as that for a GaAs sample, suggesting that the electron loses its energy primarily to the GaAs-like LO phonons in an InGaAsN sample. On the other hand, we have found that for a given laser pulse width the electron collision time is about twice as large for a GaAs sample as for an InGaAsN sample. We attribute this finding to the much larger defect density in the InGaAsN sample, as a result of, say, alloy fluctuations. This interpretation is consistent with recent experimental results on this material [10, 33].

We note that for GaAs our measured energy loss rate is substantially lower than that measured at much lower carrier densities ($\widetilde{=}$36 meV/250 fs). We attribute this difference to the reabsorption of hot phonons and/or screening of the polar-optical phonons [34] for electron density $n \widetilde{=} 10^{18}$ cm^{-3} excited in our experiments.

To obtain more information from our data, let us consider the experimental results for 1 ps laser pulse excitation. We have found that electron collision times are 22 and 10 fs for GaAs and InGaAsN, respectively. Since the photoexcited electron–hole pair density is very high ($\widetilde{=}1 \times 10^{18}$ cm^{-3}) and the defect density for the MBE-grown GaAs sample is very low ($\leqslant 10^{13}$ cm^{-3}), the 22 fs electron collision time has to primarily come from the electron–electron scattering in GaAs. Using this information, the collision time attributed to the defects in InGaAsN can be calculated to be $\tau_{\text{ele–defect}} \widetilde{=} 18$ fs, or the scattering

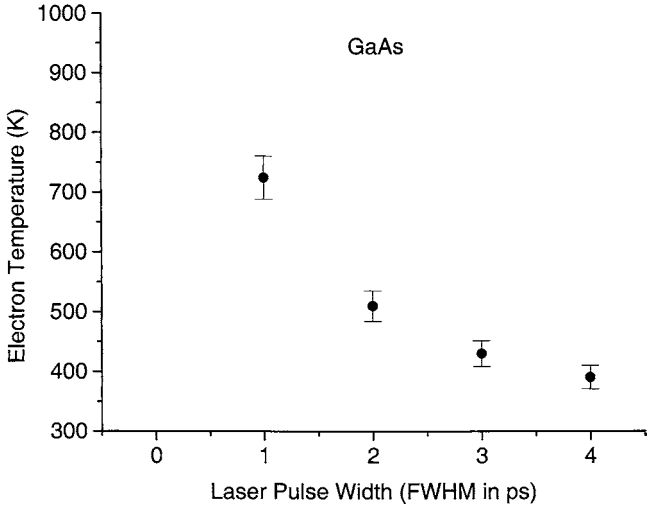

Figure 6. The deduced electron temperature is plotted as a function of the laser pulse width for a high-quality MBE-grown GaAs sample. The energy loss rate under similar experimental conditions is found to be (63 ± 6) meV ps^{-1}, indicating that electrons lose energy primarily through electron–LO phonon interactions in InGaAsN.

rate due to defects is $\Gamma_{\text{defect}} = 5.45 \times 10^{13}$ s^{-1}. Because the average electron velocity in InGaAsN is given by $\bar{v} = \sqrt{3k_{\text{B}}T_{\text{e}}/m_{\text{e}}^*} = 6.74 \times 10^5$ m s^{-1}, we obtain for InGaAsN $n_{\text{defect}}\sigma_{\text{defect}} = \Gamma_{\text{defect}}/\bar{v} = 5.45 \times 10^{13}/6.74 \times 10^5 = 8.07 \times 10^7$ m^{-1}, where n_{defect} is the defect density and σ_{defect} is the microscopic scattering cross section of the defect. Therefore, our experimental results can provide information about the defect density if the microscopic scattering cross section of the defect is known.

4. Conclusion

Non-equilibrium electron distributions and energy loss rate in an MOCVD-grown $\text{In}_x\text{Ga}_{1-x}\text{As}_{1-y}\text{N}_y$ ($x = 0.03$ and $y = 0.01$) epilayer on GaAs substrate have been studied by picosecond Raman spectroscopy. It is demonstrated that for electron density $n \cong 10^{18}$ cm^{-3} electron distributions can be described very well by Fermi–Dirac distributions with electron temperatures substantially higher than the lattice temperature. From the measurement of effective electron temperature as a function of the pulse width of the excitation laser, the energy loss rate in $\text{In}_x\text{Ga}_{1-x}\text{As}_{1-y}\text{N}_y$ is estimated to be 64 meV ps^{-1}. Within our experimental uncertainty, the electron energy loss rate has been found to be the same in InGaAsN as in GaAs, suggesting that the electron loses its energy primarily to the GaAs-like LO phonons in an InGaAsN sample. The electron collision time for GaAs has been found to be substantially larger than that for InGaAsN, indicating that the latter has much higher defect density than the former.

Acknowledgments

This work is supported by the National Science Foundation under grant No DMR0305147 and the Multi-Investigator Proposal Development Grant Program of College of Liberal Arts and Sciences at Arizona State University.

References

[1] Kondow M, Uomi K, Niwa A, Kitatani T, Watahiki S and Yazawa Y 1996 *Japan. J. Appl. Phys.* 1 **35** 1273
[2] Kondow M, Kitatani T, Larson M C, Nakahara K, Uomi K and Inoue H 1998 *J. Cryst. Growth* **188** 255
[3] Xin H P and Tu C W 1998 *Appl. Phys. Lett.* **72** 2442
[4] Miyamoto T, Takeuchi K, Kageyama T, Koyama F and Iga K 1998 *Japan. J. Appl. Phys.* 1 **37** 90
[5] Sato S, Osawa Y and Saitoh T 1997 *Japan. J. Appl. Phys.* 1 **36** 2671
[6] Sato S and Satoh S 1998 *J. Cryst. Growth* **192** 381
[7] Bellaiche L 1999 *Appl. Phys. Lett.* **75** 2578
[8] Geisz J F, Friedman D J, Olson J M, Kurz S R and Keyes B M 1998 *J. Cryst. Growth* **195** 401
[9] Friedman D J, Geisz J F, Kurz S R and Olson J M 1998 *J. Cryst. Growth* **195** 409
[10] Mair R A, Lin J Y, Jiang H X, Jones E D, Allerman A A and Kurz S R 2000 *Appl. Phys. Lett.* **76** 188
[11] Tsen K T 2001 *Ultrafast Physical Processes in Semiconductors* (*Semiconductors and Semimetals* vol 67) ed K T Tsen (New York: Academic) p 109
[12] Klein M V 1983 *Light Scattering in Solids I* ed M Cardona and G Guntherodt (New York: Springer) p 151
[13] Tsen K T 2001 *Ultrafast Phenomena in Semiconductors* ed K T Tsen (New York: Springer) p 191
[14] Kim D S and Yu P Y 1991 *Phys. Rev.* B **43** 4158
[15] Platzman P M and Wolff P A 1973 *Waves and Interactions in Solid State Plasmas* (*Supplement in Solid State Physics* vol 13) (New York: Academic)
[16] Kane E O 1957 *J. Phys. Chem. Solids* **1** 249
[17] Cohen M L and Chelikowsky J 1989 *Electronic Structure and Optical Properties of Semiconductors* (*Springer Series in Solid State Sciences* vol 75) 2nd edn (Berlin: Springer)
[18] Jha S S 1969 *Nuovo Cimento* B **63** 331
[19] Chia C, Sankey O F and Tsen K T 1992 *Phys. Rev.* B **45** 6509
[20] Chia C, Sankey O F and Tsen K T 1992 *J. Appl. Phys.* **72** 4325
[21] Chia C, Sankey O F and Tsen K T 1993 *Mod. Phys. Lett.* B **7** 331
[22] Kane E O 1957 *J. Phys. Chem. Solids* **1** 249
[23] Hamilton D C and McWhorter A L 1969 *Light Scattering Spectra of Solids* ed G Wright (New York: Springer) p 309
[24] Smekal A 1923 *Naturwissenschaften* **11** 873
[25] Kramers H A and Heisenburg W 1925 *Z. Phys.* **31** 681
[26] Raman C V 1928 *Ind. J. Phys.* **2** 387
[27] Lansberg G and Mandel'shtam L 1928 *Naturwissenschaften* **16** 57
Lansberg G and Mandel'shtam L 1928 *Naturwissenschaften* **16** 772
[28] Jackson J D 1975 *Classical Electrodynamics* 2nd edn (New York: Wiley) pp 391–7
[29] See for example, Yu P Y and Cardona M 1996 *Fundamentals of Semiconductors* (New York: Springer)
[30] Pinczuk A, Abstreiter G A, Trommer R and Cardona M 1979 *Solid State Commun.* **30** 429
[31] Kim D S and Yu P Y 1990 *Appl. Phys. Lett.* **56** 1570
[32] Kim D S and Yu P Y 1990 *Appl. Phys. Lett.* **56** 2210
[33] See for example, Hess K, Leburton J-P and Ravaioli U (ed) 1995 *Hot Carrier in Semiconductors* (New York: Plenum)
[34] Kwon D, Kaplar R J, Ringle S A, Allerman A A, Kurtz S R and Jones E D 1999 *Appl. Phys. Lett.* **74** 2830